

# Application of Genetic Algorithm to Estimate the Large Angular Scale Features of Cosmic Microwave Background

Parth Nayak<sup>1</sup> and Rajib Saha<sup>1</sup>

<sup>1</sup>*Department of Physics, Indian Institute of Science Education and Research (IISER) Bhopal, 462066, India*

Accepted XXX. Received YYY; in original form ZZZ

## ABSTRACT

Genetic Algorithm (GA) – motivated by the natural evolutionary process – is a robust method to estimate the optimal solutions of problems involving one or more objective functions. In this article, for the first time, we apply GA to reconstruct the cleaned CMB temperature anisotropy map over large angular scales of the sky using (internal) linear combination (ILC) of observations from the final-year WMAP and Planck satellite missions. To avoid getting trapped into a local minimum, we implement the GA with generous diversity in the populations. This is achieved by introducing a small but significant amount of mutation of genes during crossover and selecting pairs with diverse fitness coefficients. We find that the new GA-ILC method produces a cleaned CMB map which agrees very well with the CMB map obtained using the exact and analytical expression of weights in the ILC method. By performing extensive Monte Carlo simulations of the CMB reconstruction using the GA-ILC algorithm we find that residual foregrounds in the cleaned map are minimal and mostly tend to occupy localized regions along the central galactic plane. The CMB angular power spectrum shows no indication of any bias in the entire multipole range  $2 \leq \ell \leq 32$  studied in this work. The error in the CMB angular power spectrum is minimal as well and given entirely by the cosmic variance induced error. Our results agree well with those obtained by various other reconstruction methods by different research groups. This problem-independent robust GA-ILC method provides a flexible way towards the complex and challenging task of CMB component reconstruction in cosmology.

**Key words:** cosmic microwave background – genetic algorithm – methods: data analysis.

## 1 INTRODUCTION

The cosmic microwave background (CMB) angular power spectrum is one of the most crucial probes of the cosmological parameters and the dynamical history of the universe. The thermal radiation is observed by various satellite missions such as WMAP (Bennett et al. 2013a) and Planck (Planck Collaboration et al. 2020a). This primordial signal, however, is largely contaminated by the emissions from outside the Milky Way as well as within. These sources of contamination are collectively called the “foreground” sources since we are concerned with the cosmic microwave *background*. For instance, the hot interstellar dust inside the galaxy emits strongly at frequencies  $\gtrsim 70$  GHz. This is referred to as the dust emission and is one kind of foreground. Some other kinds of foreground are synchrotron and free-free emissions from galactic and extragalactic sources (Ichiki 2014; Bennett et al. 2003a; Bouchet & Gispert 1999; Hinshaw et al. 2003). Hence, an accurate estimation of the angular power spectrum of pure CMB from the foreground-contained observations is crucial for precision cosmology.

Since the onset of the scientific observations of CMB, extensive research has been done to come up with ways of effective foreground removal and accurate CMB retrieval. As

a consequence, several methods exist in literature for getting rid of the foreground. However, most of them make use of the underlying spectral and spatial models of the foreground (Hinshaw et al. 2003; Bennett et al. 2003b; Hinshaw et al. 2007). For example, a Gibbs sampling approach (Geman & Geman 1984) is proposed and implemented to separate CMB and foreground components by Eriksen et al. (2004a, 2007); Eriksen et al. (2008a,b); and a maximum likelihood approach to reconstruct CMB and foreground components using prior noise covariance information and foreground models is implemented by Eriksen et al. (2006); Gold et al. (2011). However, they may have uncertainties arising due to incomplete information of the foreground frequency and spatial dependence (Dodelson 1997; Tegmark 1998). A completely model-independent method is the internal linear combination (ILC) of multifrequency observations (Tegmark & Efstathiou 1996). Sudevan & Saha (2018a) explore the CMB posterior using a Gibbs sampling approach within a global ILC framework. Sudevan & Saha (2018c) study the method in the wake of the theoretical CMB covariance information. All these works have been carried out considering the Gaussian nature of the primordial anisotropy signal; any non-Gaussianities are small fluctuations (Allen et al. 1987; Falk et al. 1992; Gangui et al. 1994; Acquaviva et al. 2003; Maldacena 2003). Saha

(2011) considers the highly non-Gaussian inheritance of the foreground emissions and proposes an ILC method to get rid of the non-Gaussian contamination based on the kurtosis minimization. Other notable studies of the ILC method include, but not limited to, Tegmark et al. (2003); Bennett et al. (2003b); Eriksen et al. (2004b); Saha et al. (2006, 2008a). Some of the previous works also suggest that, depending on the context of the underlying problem, an exact analytical ILC solution may not be possible to find.

We propose an expression-independent, numerical ILC technique for a robust and effective CMB foreground reconstruction. In this work, we apply the novel numerical method over the global ILC proposed by Sudevan & Saha (2018c), making use of the Planck mission’s theoretical CMB angular power spectrum (Planck Collaboration et al. 2020c) in our computation of the reduced variance of the output map. We apply the genetic algorithm (GA) for estimating optimal ILC weights to produce a clean map. An evolutionary algorithm such as this involves several inherent parameters that need to be studied extensively for such an implementation. For our study of the method over the large angular scales, we make use of the low-resolution WMAP and Planck observations as input at HEALPix<sup>1</sup>  $N_{\text{side}} = 16$ . We smooth the input maps by a Gaussian beam at 9° FWHM. Presumably, this also reduces the pixel-uncorrelated noise level (which is dominant on smaller angular scales).

We perform detailed Monte Carlo simulations to ensure the statistical sanity of our method. We find that this novel GA-ILC method produces a clean map with a minimal residual foreground. The residuary contamination tends to occupy small localized regions close to the galactic plane. The angular power spectrum of the clean map contains no apparent bias in the multipole range of  $2 \leq \ell \leq 32$ . The reconstruction errors in the angular power spectrum are also minimal and conform to the cosmic variance-induced errors.

The organization of this paper is as follows. We describe the basic formalism of the method in section 2. We elaborate on the exact implementation of this method in section 3. We present our trial GA implementation for validation in section 4. We discuss the GA-ILC implemented with Monte Carlo simulations in section 5. We present the results obtained by using the techniques of this work on WMAP and Planck final-year data and discuss our findings in section 6. We conclude our paper by outlining some key aspects of this work and its future prospects in section 7.

## 2 FORMALISM

Suppose there are  $N$  channels of different frequencies, each producing a temperature anisotropy map (hereinafter simply, “map”) upon observation. A map observed from the  $i$ th frequency channel is denoted by the vector  $\Delta\tilde{\mathbf{T}}_i$  in the HEALPix pixelated format. The size of this vector is  $p \equiv N_{\text{pix}} = 12N_{\text{side}}^2$ .

Since a map is defined over a sphere, it can be expanded

in the so-called “harmonic space” as

$$\Delta\tilde{\mathbf{T}}_i(n) = \sum_{\ell m} a_{\ell m}^i Y_{\ell m}(n), \quad (1)$$

where  $n$  denotes the pixel index (corresponding to some direction vector  $\hat{\mathbf{n}}$ ),  $Y_{\ell m}$  are the standard spherical harmonics, and  $a_{\ell m}^i$  are called the harmonic coefficients of the  $i$ th map. The multipole index  $\ell$  is of special importance because it indicates the underlying angular scale ( $\theta_\ell \sim 2\pi/\ell$ ). The cross-correlation of the harmonic coefficients of maps  $i$  and  $j$  is also called the cross power spectrum, defined by

$$C_\ell^{ij} = \sum_{m=-\ell}^{\ell} \frac{a_{\ell m}^{i*} a_{\ell m}^j}{2\ell + 1}. \quad (2)$$

The auto-correlation of the harmonic coefficients of the  $i$ th map is called its angular power spectrum,  $C_\ell^i$ . The CMB angular power spectrum is the single, most important quantity we would like to accurately estimate by finding an optimal clean CMB map from multifrequency observations. All observed maps consist primarily of CMB and foreground. Various foreground emissions are not thermalized, hence, they do not have a blackbody spectrum unlike CMB, which follows the thermal blackbody distribution with great accuracy (Mather et al. 1994). Hence, across different frequency bands, the thermodynamic temperature of the foreground patches varies whereas the CMB temperature will be constant. ILC exploits this fact as a benefit of multifrequency observations.

Apart from foreground, detector-noise is also one of the components that contaminates the observed CMB signal. Although small amount of noise is present on all angular scales, it is dominant only on the smaller angular scales of the data which are irrelevant for this work. Furthermore, noise from any two frequency channels is uncorrelated (Hinshaw et al. 2003, 2007; Jarosik et al. 2003, 2007), more to the advantage of ILC.

An observed CMB map in  $i$ th frequency channel can thus be expressed as

$$\Delta\tilde{\mathbf{T}}_i = \Delta\tilde{\mathbf{T}}_{\text{CMB}} + \Delta\tilde{\mathbf{T}}_{\text{fg},i} + \Delta\tilde{\mathbf{T}}_{\text{noise},i}. \quad (3)$$

Notice that the CMB part,  $\Delta\tilde{\mathbf{T}}_{\text{CMB}}$ , does not contain an  $i$  index since the CMB temperature is independent of frequency.

### 2.1 Internal Linear Combination

Tegmark & Efstathiou (1996) proposed a model-independent method to estimate the clean CMB signal from a multifrequency observation. ILC attempts to find the optimal estimate of CMB from multifrequency foreground-contaminated maps without using any external templates or models. In this technique, we start by writing a linear combination of  $N$  multifrequency input maps to find a clean output map. This is simply

$$\mathbf{P} \equiv \Delta\tilde{\mathbf{T}}_{\text{clean}}(\{w_i\}) = \sum_{i=1}^N w_i \Delta\tilde{\mathbf{T}}_i, \quad (4)$$

where  $\{w_i\}$  are the coefficients, more commonly called the *weights* given to all the input maps before summing them.

<sup>1</sup> Hierarchical Equal Area isoLatitude Pixelation of sky, e.g., see Górski et al. (2005)

Using Eqn. (3), this yields

$$\mathbf{P} = \left( \sum_{i=1}^N w_i \right) \Delta \tilde{\mathbf{T}}_{\text{CMB}} + \sum_{i=1}^N w_i \Delta \tilde{\mathbf{T}}_{\text{trash},i}, \quad (5)$$

where  $\Delta \tilde{\mathbf{T}}_{\text{trash},i} = \Delta \tilde{\mathbf{T}}_{\text{fg},i} + \Delta \tilde{\mathbf{T}}_{\text{noise},i}$ . In order to preserve the norm of the clean CMB map, a constraint is imposed in the form

$$\sum_{i=1}^N w_i = 1 \quad \text{or} \quad \mathbf{e}^T \mathbf{w} = 1, \quad (6)$$

where  $\mathbf{e} = (1, 1, \dots, 1)^T$  is the column vector of size  $N$  with all entries 1. In the usual ILC method, the best estimate of CMB is obtained by minimizing the variance of the clean map,  $\mathbf{P}^T \mathbf{P}$ , w.r.t. the choice of the weight vector,  $\mathbf{w}$ . This is a problem of multivariable constrained optimization and the analytical solution can be found by using the Lagrange's multipliers method (e.g., see Tegmark & Efstathiou (1996); Saha et al. (2008b)) as,

$$\mathbf{w}_{\text{usual}} = \frac{\mathbf{e}^T \mathbf{C}^{-1}}{\mathbf{e}^T \mathbf{C}^{-1} \mathbf{e}}, \quad (7)$$

or following summation notation,

$$w_{\text{usual},i} = \frac{\sum_{j=1}^N C_{ij}^{-1}}{\sum_{i',j'=1}^N C_{i'j'}^{-1}}, \quad (8)$$

where  $\mathbf{C}$  is the  $N \times N$  square symmetric covariance matrix of the  $N$  input maps. In case the covariance matrix is singular, it is possible to generalize the inverse as the Moore-Penrose pseudoinverse (Moore 1920; Penrose 1956)  $\mathbf{C}^{-1} \mapsto \mathbf{C}^\dagger$ . If  $\mathbf{C}$  is not singular,  $\mathbf{C}^\dagger = \mathbf{C}^{-1}$ . Rewriting Eqn. (7) in terms of the pseudoinverse,

$$\mathbf{w}_{\text{usual}} = \frac{\mathbf{e}^T \mathbf{C}^\dagger}{\mathbf{e}^T \mathbf{C}^\dagger \mathbf{e}}. \quad (9)$$

Sudevan & Saha (2018c) (SS, for short) proposed a new, global ILC method making use of the prior knowledge of the theoretical covariance of CMB. The method employs this additional information to assert that the covariance structure of the final clean map is consistent with the expectation of pure CMB. Instead of minimizing the variance of the clean map, this global ILC seeks to minimize the reduced variance, called  $\sigma^2$ , calculated as

$$\sigma^2 = \mathbf{P}^T \mathbf{C}_{\text{th}}^\dagger \mathbf{P}, \quad (10)$$

where  $\mathbf{C}_{\text{th}}$  is the theoretical CMB *pixel-pixel* covariance matrix of size  $p \times p$  and  $\dagger$  represents the pseudoinverse. From the definition of  $\mathbf{P}$  in Eqn. (4), we can write

$$\sigma^2 = \mathbf{w}^T \mathbf{A} \mathbf{w}, \quad (11)$$

where  $\mathbf{A}$  is an  $N \times N$  square matrix with elements

$$A_{ij} = (\Delta \tilde{\mathbf{T}}_i)^T \mathbf{C}_{\text{th}}^\dagger \Delta \tilde{\mathbf{T}}_j. \quad (12)$$

Similarly to the usual ILC, using the Lagrange multipliers with the same constraint, the optimal weights under this global ILC can be found as

$$\mathbf{w}_{\text{SS}} = \frac{\mathbf{e}^T \mathbf{A}^\dagger}{\mathbf{e}^T \mathbf{A}^\dagger \mathbf{e}}. \quad (13)$$

As found by Sudevan & Saha (2018b), the matrix  $\mathbf{A}$  can

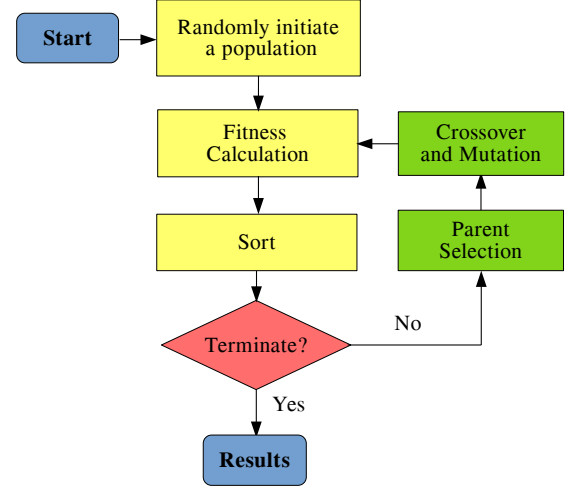


**Figure 1.** The flowchart of a typical GA. The sorting is introduced in order to ensure the better readability and presentability of the solutions in a population.

be calculated as

$$A_{ij} = \sum_{\ell=2}^{\ell_{\text{max}}} (2\ell + 1) \frac{C_{\ell}^{ij}}{C'_{\ell,\text{th}}}, \quad (14)$$

where  $C'_{\ell,\text{th}}$  is the theoretical power spectrum of CMB after accounting for the beam and pixel effects, *i.e.*

$$C'_{\ell,\text{th}} = C_{\ell,\text{th}} B_{\ell}^2 P_{\ell}^2, \quad (15)$$

where  $B_{\ell}$  are the Legendre transforms of the beam function and  $P_{\ell}$  are the HEALPix pixel window functions.  $\ell_{\text{max}}$  can be chosen according to the pixel angular resolution of the maps. In this work, we made use of the low resolution maps at  $N_{\text{side}} = 16$ , for which  $\ell = 32$  is a sufficiently large multipole. The sum is taken starting from  $\ell = 2$  because the monopole ( $\ell = 0$ ) and dipole ( $\ell = 1$ ) are uninteresting for cosmological studies, and hence, they are removed from the input maps prior to all the analyses.

## 2.2 Genetic Algorithm

Genetic algorithm (GA) was first proposed by John H. Holland (Holland 1962) in the mid 1960s and was further extended by David Goldberg in the late 1980s (Goldberg 1989). GA aims to find global optimal solution(s) to objective functions having a multimodal nature, *i.e.*, it has multiple local optima in the domain of search. As the conventional optimization algorithms tend to fail in such cases, GA opens up a new window with its novel concept. The underlying principle of GA is Darwin's theory of "natural selection". The biological species evolve by this natural process. In a population, each individual has a different set of genetic characteristics. Thus, the whole population has a diverse gene pool. This community is subject to certain natural circumstances known as the environment. The process of natural selection asserts that the genes which lead to better traits for survival will more likely be passed on to the offspring by reproduction over the generations than those which do not. Occasional mu-

tations may bring in new beneficial genes that were earlier not present. Hence, eventually the whole population will best adapt to its environment after several generations.

GA employs this strategy to the optimization problems. The goal at hand is to numerically find the global optimum of an objective function in the given domain of interest. GA works on the principle of convergence with variation. Diversity in a population is a necessary ingredient for the GA to succeed. Over the generations, individual solutions with higher and higher fitness dominate the population. Fig. 1 shows the flowchart of a typical GA. In the following we briefly discuss the most common steps of GA.

(i) Population initialization: GA derives from the basic ideology of population genetics. Hence, GA is based on a “population” – a set of possible solutions to the problem. According to the domain of search for the optimal solution, a population can be randomly created. The size of a population is a heuristic parameter.

(ii) Fitness calculation: A fitness function is chosen such that the fitter individuals will be closer to the optimum (in the functional space) than the less fit ones. The choice of a fitness function depends on the underlying objective and it is not unique. However, in order for a proper implementation of the algorithm, the fitness function should be positive and analytic, at least in the domain of interest.

(iii) Parent selection: This is one of the most crucial steps of the entire algorithm. As Natural selection dictates, the fitter individuals in the population are more likely to pass on their genes by mating than the less fit ones. To simulate this scenario, we must assign some weights to the individuals according to their fitness. One most common method is the fitness-proportionate assignment of weights (probabilities). In this step the pairs are selected for mating and producing the new generation. There is a set of methods for this. We will discuss some of them in section 3.

(iv) Crossover and Mutation: From the parents selected in the previous step, we now make crossovers to generate new individuals, collectively called “offspring”. The new individuals are occasionally mutated with a small amplitude. In our case, mutation refers to a discrepancy in the passage of genes from one generation to the next. Mutation is a crucial tool to bring in variety in the genetic material. We discuss the importance of mutation in section 3. The offspring thus produced will constitute the next generation of our population.

(v) Termination: Steps (ii)-(iv) are repeated in a loop for each new generation until the stopping criteria are reached/GA has “converged”. In general, a GA implementation is said to have converged if the fitness of the best individual(s) over the generations does not improve any further. The programmer can set a stop-point generation, hitting which will end the generation loop. This stop-point can be found by *hit-and-trail*. Altogether, the fittest individual in the last generation is deemed the solution of the GA run.

Fig. 2 uses a toy-model population to visually understand the different terms and steps in our GA implementation. (We discuss it further in the due course.) In section 3, we describe the methodology adopted for this implementation of GA-ILC with the details concerning the exact styles and the values of certain parameters.

### 3 METHODOLOGY

Python is one of the most commonly used programming languages for scientific computation. It provides many open-source packages for various utilities. One of those packages is the python-port of HEALPix, HEALPy. It comes with many utilities we need for handling and analyzing the data. There are pixel utilities, spherical-harmonic transform utilities, visualization related functions and many miscellaneous tools for an effective manipulation and reduction of a HEALPix data-set. We have implemented the algorithm in Python 3 for numerical computations.

In this work, GA is implemented to find the optimal weights to linearly combine the input maps such that the reduced variance of the clean map is minimized. This is a multivariable constrained optimization problem. In the present work, the problem is converted to an unconstrained optimization problem by a little manipulation of the method. The objective function to be optimized (minimized) is the (reduced) variance function (Eqn. (11))

$$\sigma^2(\mathbf{w}) = \mathbf{w}^T \mathbf{A} \mathbf{w}. \quad (16)$$

The constraint is  $\sum_{i=1}^N w_i = 1$ . Alternatively, for the current work, one of the  $N$  weights is found as  $w_{i'} = 1 - \sum_{i \neq i'} w_i$ . (It is the last weight of the spectrally-ordered system for our work.) Thus, the goal is to estimate  $\mathbf{w}_{\text{GA}}$  that minimize  $\sigma^2(\mathbf{w})$  using GA.

#### 3.1 Implementation of GA-ILC

In Genetics, an individual can be represented by its genotypic as well as phenotypic characteristics. In our GA, the phenotype of an individual is a decimal number in the case of a single variable problem and a vector (array) of  $n$  decimal numbers in the case of a multivariable problem. We chose the binary-string representation as our genotype. The required decimal accuracy is a fixed parameter initially chosen by the programmer. Depending upon the accuracy, each individual fraction can be converted to an integer by multiplying it with  $10^{\text{decimal-accuracy}}$  and rounding off. Then the integer is converted into its binary representation. In the multivariable cases, each element of a vector is converted into a binary string and all of those strings are concatenated in the original order into a single large string. We call this string a “chromosome”. The binary part of an individual element of this vector chromosome is called a “segment”, each position of a chromosome is called a “gene”, and the bit-value of each gene is called the “allele” of that gene. Fig. 2 (A) depicts a schematic of this terminology. It shows an example one-variable population in the genotype representation. By performing the exact inverse operations on a chromosome will return the phenotype (decimal vector) of that individual.

Now that the terminology is clear, we need to initialize a population. The size of the population,  $\text{Popsize}$ , is fixed by the programmer by *hit-and-trial*. A domain of search must be first decided. For our GA-ILC, we chose  $\{w_{\text{SS},i} \pm 1\}$  as the domain, hereinafter called “priors”. The initial population is then uniformly randomly generated. The population at any stage of calculation is a 2D array with one dimension containing genes of a single chromosome and the other containing as many as  $\text{Popsize}$  chromosomes. The allele of each gene of each chromosome is determined by generating a

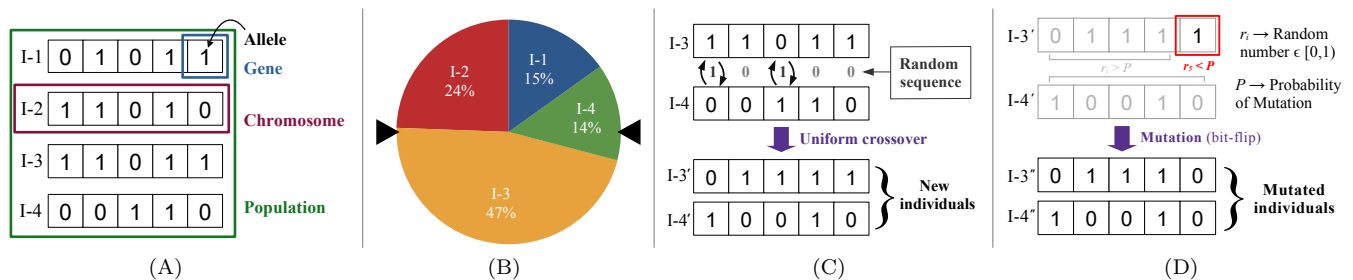


**Figure 2.** A schematic representation of a toy-model of GA. (A) shows a population with 4 individuals and indicates the terminology within a GA framework. (B) shows a Roulette wheel with two fixed-points diametrically opposite pointing to I-3 and I-4. (C) shows a typical uniform crossover event on I-3 and I-4, producing the new individuals I-3' and I-4'. These are the offspring which then get mutated into I-3'' and I-4'' as shown in (D). All the numbers including binary strings and probabilities are only meant for visualization of this toy-model.

(pseudo-) random number between 0 and 1, and according to whether it is less or greater than  $1/2$ . This is, in some sense, the coin-toss determination and it is frequently used in this work. From the binary population, the decimal population is also found. At this point a check is made on whether all the variables in each individual fall within the priors imposed. The number of variables in our GA-ILC,  $N_{\text{var}}$ , is one less than the number of input maps since one of the weights is dependent on the rest of them.

A suitable fitness function for the GA-ILC is chosen as

$$\bar{f}(\mathbf{w}) = \frac{1}{\sigma^2(\mathbf{w})}. \quad (17)$$

Since the  $\sigma^2$  is strictly positive, this fitness function satisfies the criteria of being a positive analytic function (in principle, the global minimum of  $\sigma^2$  is the reduced variance of a pure CMB map).

As discussed in subsection 2.2, there are various methods for selecting parent pairs from a given fitness-associated population. Some of them are the fitness-proportionate selection methods which assign weights proportional to the fitness of the individuals, whereas some make use of the fitness values indirectly in doing so. One of the most common parent selection methods (which we use in this work) is called ‘‘Stochastic Universal Sampling’’ or ‘‘SUS’’ in short. It is a Roulette-wheel-based method in which, depending upon the number of individuals to be picked in one turn of the wheel, there is a number of fixed-points. In case of picking pairs, there are two fixed-points, equally separated around the wheel’s periphery. A turn of the wheel is simulated by generating a pseudorandom number.

In a fitness-proportionate (‘‘FP’’ for short) selection of parents, the area assigned to each individual in a population on the wheel is directly proportional to their fitness. Thus, depending upon the number of pairs to be picked (a.k.a. size of the ‘‘mating-pool’’), the wheel is turned so many times and each turn will return two individuals as a pair. This scenario of fitter individuals having better chance of reproduction is dubbed the ‘‘selection pressure’’. However, as the generations progress and the population approaches the desired optimum, the fitness value may get less and less diverse due to a decreasing gradient of the objective function. In such cases, the selection pressure to the fitter individuals wanes since all the individuals will be assigned an *almost* equal area on the wheel. To make sure this does not happen, another selection method such as ‘‘Rank selection’’ can be employed. In

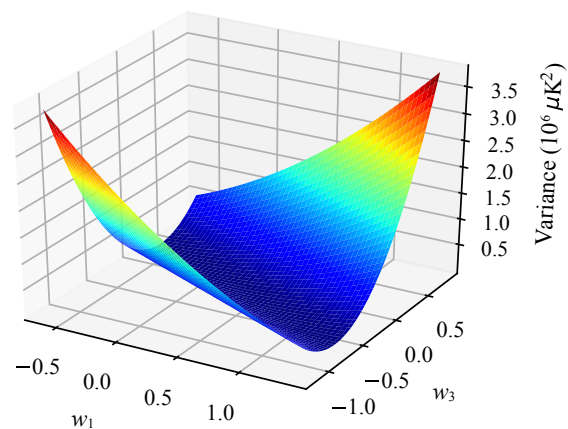


**Figure 3.** The variance function in Eqn. (16) plotted against two weights  $w_1$  and  $w_3$  while keeping the rest of the weights fixed to the SS weights. This is performed on the simulation of seed 100 low-resolution maps. A very broad valley can be seen close to the supposed global minimum.

this technique, the individuals in the population are sorted according to their fitness values and they are assigned ranks. Then the weights are assigned according to their ranks, irrespective of their fitness values. Nonetheless, the individual(s) with the highest fitness value will have the largest weight. The selection is then done by the Roulette-wheel turnings. This method brings the selection pressure back into the picture as the weight-gradient is preserved. When the objective function in the domain of search inherently has a less gradient, rank selection should be preferred from the start of the generation loop. If closer to the optimum point the function is less steep, then after a certain number of generations the selection type can be switched from FP to rank selection. This switching-point generation is another GA parameter called `switch`. Fig. 2 (B) shows a Roulette wheel in our toy-model population with some area given to all four individuals under either of the selection settings. Notice that the two fixed-points for picking pairs are diametrically opposite to each other. This way, an individual with low selection pressure may also get picked occasionally, maintaining the genetic diversity in GA.

The variance function in Eqn. (16) is plotted in Fig. 3 for a pair of weights while keeping the rest of the weights fixed

to the SS-weights. It is done on one of the realizations in the Monte Carlo simulations we performed (we discuss it further in section 5). As can be seen in that figure, the variance function has a very broad valley close to the global minimum. We verified that the feature is present irrespective of the pair of weights chosen. This required us to switch between FP and rank selection types after a `switch-point` generation. It is yet another parameter that must be fixed by *hit-and-trial* like all the rest of the GA parameters and is variable for a plethora of GA implementations.

The crossover again comes with a variety of types. Some of the most popular types are one-point, two-point,  $k$ -point, uniform crossovers. We chose the uniform crossover as the universal type for our entire work. An instance of this type of crossover is schematically shown in Fig. 2 (C) for our toy-model population. Under uniform crossover, the alleles of each gene are exchanged between the two parent chromosomes of a pair using the coin-toss determination technique. Thus, each pair of parents give rise to a pair of children. These children are mutated with a small amplitude, `P_mut`. A mutation is introduced as the following. For each gene of each child chromosome, a pseudorandom number  $r$  in the range  $[0, 1)$  is generated. If  $r < P\_mut$ , the allele of that gene is flipped ( $0 \rightarrow 1$  and  $1 \rightarrow 0$ ). The parameter `P_mut` is best chosen by the programmer by *hit-and-trial*. Fig. 2 (D) indicates one of the mutation incidents in the toy-model GA. After these steps, we have a set of offspring chromosomes at hand. Depending upon the fitness of the children and the size of the population, a new generation is recruited by keeping `Popsize`-many fittest children into the population and discarding the rest of them. The newly deemed population will then undergo the same steps of parent selection and mating. Proper termination criteria in terms of the number of generations, `N_gen`, is found by observing the convergence of GA-ILC and subject to the computational resources.

### 3.2 Remarks on Genetic Diversity

It is particularly important to ensure a genetically diverse population at *each* step of GA. The initial population is randomly initialized to have the maximum diversity possible. While applying selection pressure towards the fitter individuals, the less fit individuals should not be neglected entirely. A balanced reproduction is only possible if the entire population takes part in mating. We need to make sure that the least fit individuals also get to reproduce at least a couple times. A way to ensure this (in addition to using SUS method) is to make  $N\_pairs \sim \lceil 1/(\min(\{p_i\})) \rceil$  where  $\{p_i\}$  is the set of probabilities (weights) assigned to the individuals and  $\lceil \cdot \rceil$  is the ceiling function. If this is less than half `Popsize`, `N_pairs` can simply be `Popsize`. Due to the limited resources and increasing requirement of computing power, the bottleneck must be applied to filter-out the fitter individuals after reproduction and preserve the size of the population at each generation. This results in only a *slightly* reduced genetic diversity, which is harmless considering the variety of children produced by mutation. Mutation, thus, is a very crucial ingredient in our GA. Indeed, a mild mutation prevents GA from premature convergence. A GA-ILC implementation without any mutation loses the genetic diversity almost completely as it moves towards the global optimum and causes it to converge to some false local optimum which is not ac-

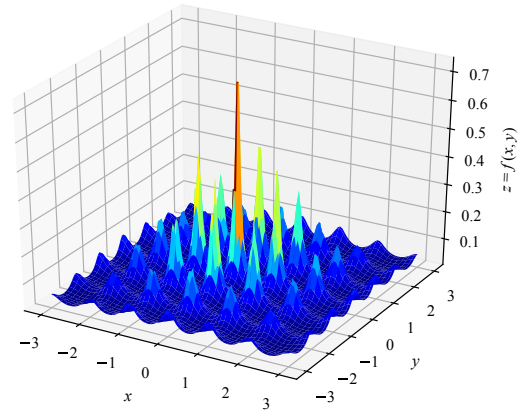


**Figure 4.** The two-variable case of the trial function in Eqn. (18) within an appropriate domain of interest. Observe the highly multimodal nature with multiple local maxima located closely together.

tually present. It is a partly computational – partly fundamental defect (in that a non-diverse, self-breeding population eventually ceases to survive under natural selection). In Population Genetics, occasional mutation may, by pure chance, introduce a better trait for survival and is preferred through generations. We studied this very interesting ingredient in more detail in our work. We discuss this further in sections 5 and 6.

## 4 VALIDATION OF THE GA IMPLEMENTATION

Implementation of GA is a complicated task. In particular, the programmer needs to find the optimal values of various GA parameters mostly by *hit-and-trial* as mentioned quite frequently throughout subsection 3.1. The most common GA parameters are the population size `Popsize`, number of total generations `N_gen`, decimal accuracy required `Dec`, probability of mutation `P_mut`, etc. Hence, it is wise to start with a very simple implementation and then move towards more complicated problems. We have employed this strategy for this work. We initially implemented GA for single variable test-problems. Then we moved on to multivariable test-problems and we obtained satisfactory results in both of them. The test function we chose is

$$f(\mathbf{x}) = \frac{1}{1 + \sum_{i=1}^{N_{\text{var}}} [x_i^2 + 10(\cos(2\pi x_i) - 1)]}, \quad (18)$$

with the same function as the fitness function. This function is well-defined for any number of variables. The two-variable case of this function is shown in fig. 4 for visualization. It is observed from the figure that this trial function is a highly multimodal function *i.e.* it has multiple local maxima with a single global maximum at  $\mathbf{x} = \mathbf{0}$  with  $f(\mathbf{0}) = 1$ , within the domain of interest as plotted therein. Also, it is a steep function with large gradient. Hence, for such implementations, no mutation was necessary (in other words, `P_mut` = 0) and after  $\sim 60\%$  of total generations, the selection type was switched from FP to rank selection to compensate for having no mutation. The best of those results for different  $N_{\text{var}}$  are

**Table 1.** Results of the trial implementation for different number of variables. Notice that, for larger and larger number of variables, to get the best results, we need to have a larger and larger population.

$N_{\text{var}}$	Popsi	N_gen	Best $f(\mathbf{x}^*)$
1	200	60	1.0
2	200	60	1.0
5	400	200	1.0
10	600	250	1.0
11	600	250	1.0
12	600	250	1.0

**Table 2.** Variation of the final function value (in the trial implementation) *w.r.t* Popsi for fixed number of generations N\_gen = 250 and  $N_{\text{var}} = 11$ . Notice the very bad function value for small Popsi.

Popsi	Best $f(\mathbf{x}^*)$
400	0.5011925167207855
450	1.0000000000000000
500	0.9999999999980158
550	0.9999999999682601
600	1.0000000000000000
650	1.0000000000000000

summarized in table 1. Table 2 shows the results obtained for the fixed number of variables in the trial function – which is the same as that in our GA-ILC implementation – with different population sizes. As expected, the best function value improves as we increase the size of the population. The results of the trials as discussed here are sufficient to conclude that our GA implementation is robust and accurate in the multivariable scenario of our GA-ILC method, and that it is safe and desirable to incorporate ILC with it in the manner described in section 3.

## 5 MONTE CARLO SIMULATIONS

As a statistical test for our GA-ILC method, we performed Monte Carlo simulations using WMAP and Planck simulated maps. From the satellite missions’ observed angular power spectra, using HEALPix IDL<sup>2</sup> routine `isynfast`, anisotropy maps were randomly generated by passing an argument called `seed` which seeds the pseudorandom number generator. The sample size of our simulations is 200, with `seed` varying from 1 to 200 in steps of 1. A total of 12 low-resolution maps at  $N_{\text{side}} = 16$  were generated for each `seed` as input of GA-ILC. Of the 12 input maps, the 5 WMAP frequency bands are K (23 GHz), K<sub>a</sub> (33 GHz), Q (41 GHz), V (61 GHz), W (94 GHz); and the seven Planck frequency bands are 30, 44, 70, 100, 143, 217 and 353 GHz. These simulated maps are 9°beam-smoothed. Corresponding to each `seed`, a pure CMB map was also generated using the same routine from the Planck theoretical angular power spectrum. These CMB maps were used as references to compare with the clean maps that GA-ILC produced. Some of the GA parameters were

<sup>2</sup> IDL is the interactive data language for Unix and Linux based systems, see, e.g., <https://caligari.dartmouth.edu/doc/idl/>

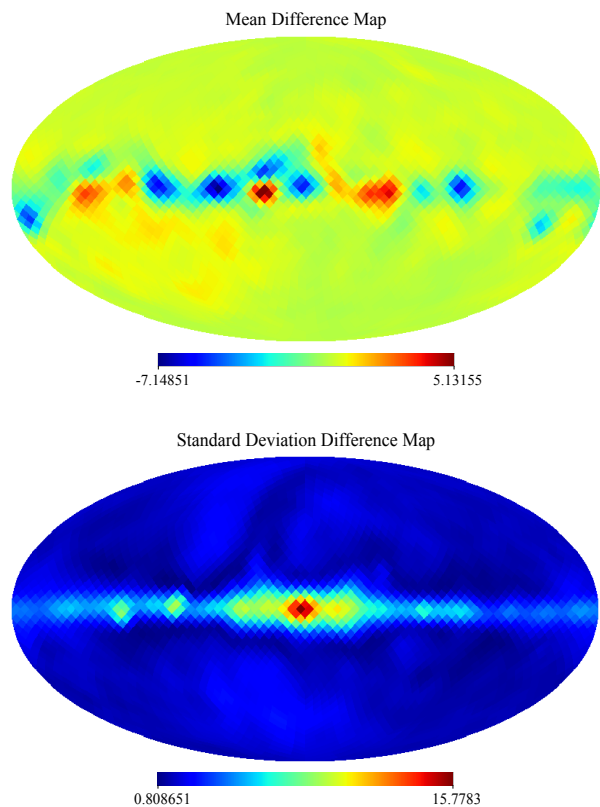


**Figure 5.** The statistical difference maps from the Monte Carlo simulations. Only a very small residual contamination seems to be present, only close to the plane of Milky Way. The unit of the values is  $\mu\text{K}$ .

kept fixed for the simulations, namely, Popsi = 400, N\_gen = 400, decimal accuracy Dec = 7, and switching between FP and rank selection types after `switch` generation # 20, all of them optimally chosen. To explore the effect of mutation on the results, GA-ILC was run for 128 different values of P\_mut starting from 0.05% in steps of 0.05%, for each `seed` value. The best results (of all P\_mut) for every `seed` were compiled and then we found the statistical measures. In particular, we found the best map of all P\_mut for every `seed` and subtracted the pure CMB simulated map for that `seed` from it. This map is called a simulated difference map here. 200 such simulated difference maps were produced and the mean and standard deviation difference maps were calculated from it. Fig. 5 shows these statistical maps. The mean difference map contains very small amount of residual contamination and that is limited to small regions around the galactic equator, as can also be inferred from the standard deviation difference map.

The angular power spectrum corresponding to the simulated mean clean map along with the standard deviation errors is overplotted with the Planck theoretical CMB power spectrum in the top panel of fig. 6. In the middle panel of the figure, the mean difference power spectrum is plotted with the errors in the estimation of mean ( $\sigma_{\mu, \ell}$ ). We observe that the estimated power spectrum is within a  $3\sigma_{\mu}$  deviation to the theoretical CMB power spectrum. This confirms that there is no bias in the entire multipole range  $2 < \ell < 32$  under

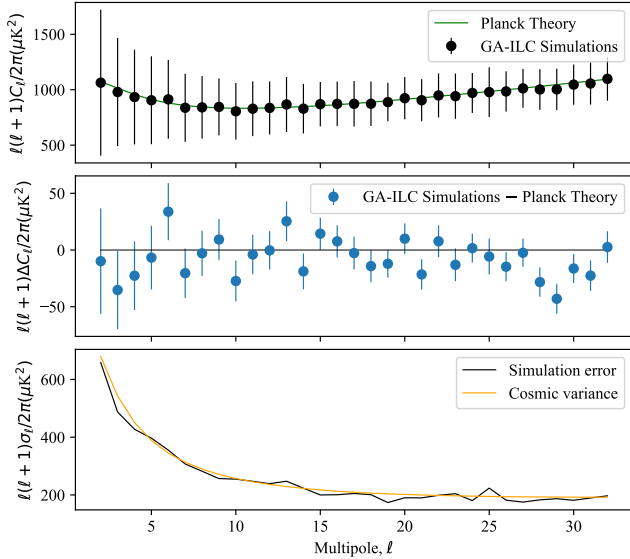


**Figure 6.** The angular power spectrum of the GA clean simulated mean difference map overlotted with the Planck theoretical power spectrum. Note that the beam and pixel effects are removed. Middle: The difference of the power spectra of GA simulations and Planck theory with errors in mean-estimation. It can be seen that the deviation is within  $3\sigma_\mu$  level which indicates that there is no bias. Bottom: The standard deviation errors in the angular power spectrum of the final mean difference map. Notice that these errors conform with the minimal errors induced by the cosmic variance,  $\Delta C_{\ell,cv} = \sqrt{\frac{2}{2\ell+1}} C_\ell$ .

study. In the bottom panel of the same figure, the standard deviation errors ( $\sigma_\ell$ ) are overlotted with the cosmic-variance induced errors. The observed errors also agree well with the expected minimal errors purely of the cosmic origin.

## 6 APPLICATION ON WMAP AND PLANCK DATA

We applied our GA-ILC on 12 multifrequency low-resolution input maps observed by WMAP and Planck to find an optimal clean map as output (we refer to this as the implementation on “data” as shorthand; the 12 input frequencies are those mentioned in section 5). GA parameters like `Popsize`, `N_gen`, `Dec`, and `switch` were kept at the fixed values, same as the Monte Carlo simulations. Similarly to the simulations, we applied GA-ILC with 144 values of `P_mut`, from 0% to 7.15% in steps of 0.05%, to analyze the final reduced variance in each case. The best case of all these 144 was deemed to represent the best version of our GA-ILC. The plot of final reduced variance against the mutation probability is shown in fig. 7. As we can see from there, a very low (or negligible) mutation does not help in our pursuit of optimization, and a large amount of mutation is also not useful. A moderately small value of 1.15% is the best mutation value in this case. There is no exact analytical problem-based expression for the optimal amount of mutation as is demonstrated by this figure. We plotted the variance values against the cumulative individuals through generations (the population is sorted in the ascending order of fitness). This type of plots are called

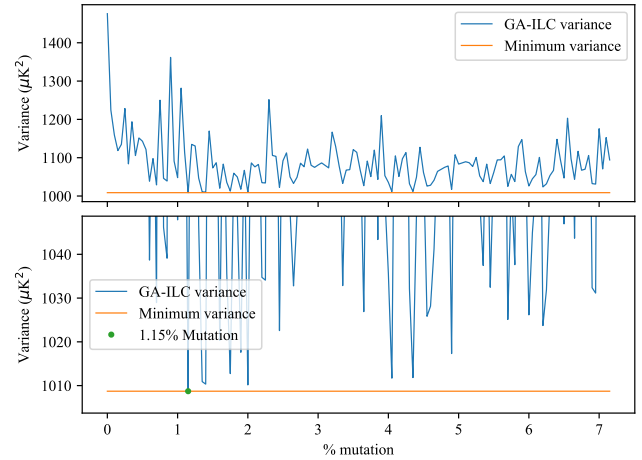


**Figure 7.** The minimal variance obtained by GA-ILC on data against the coefficient of mutation. The minimum of these minimal values – that occurs at a low-to-moderate mutation by 1.15% – is also shown distinctively. Bottom: a zoomed-in version for a closer look at the variation.

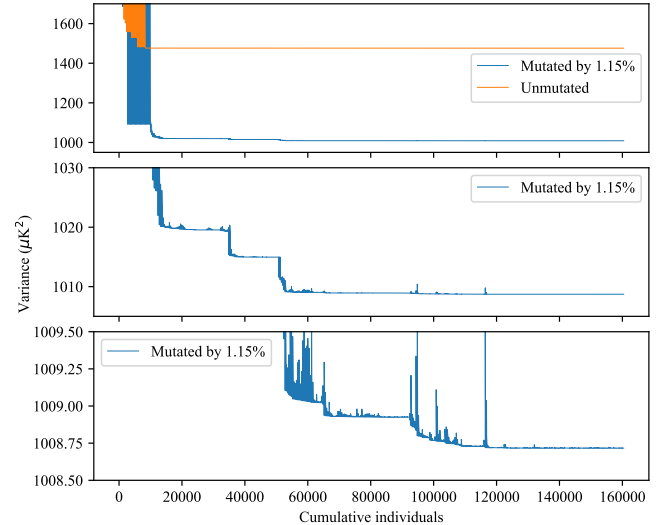
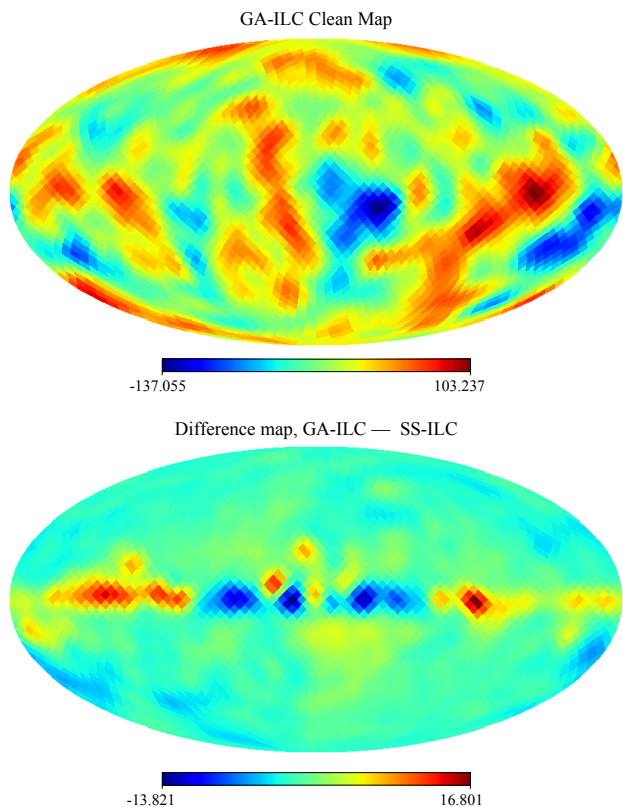


**Figure 8.** Top: The overplot of the traces of mutated and unmutated cases. The mutated case is the best among all the 144 mutation values with `P_mut` = 1.15% implemented on data. Middle and Bottom: closer look at the convergence in the mutated case.

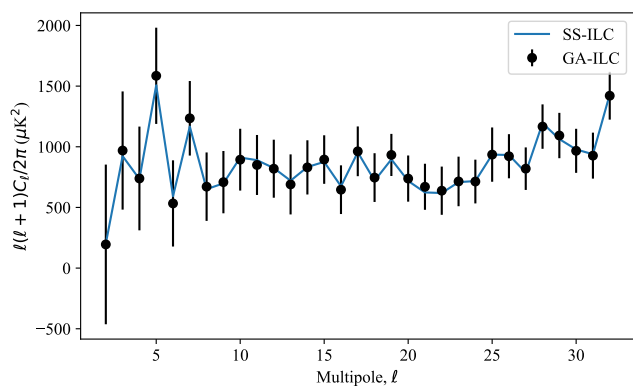
“trace-plots” here. These plots help us understand the convergence of GA and the effects of various parameters on it. Fig. 8 shows an example of trace-plots. Therein we can see that the population without any mutation converges prematurely due to the loss of genetic diversity as there exists a broad valley close to the global optimum. On the other hand, the optimally mutated case is able to find better solutions since it is able to explore the variable space. It is also evident that even when the unmutated case has long since converged, the mutated case is slowly able to find better and better solutions after generations.

Fig. 9 shows the clean CMB map produced by GA-ILC on data. Therein the bottom panel shows the difference map of GA-ILC and SS-ILC (Sudevan & Saha 2018c). It confirms





**Figure 9.** The clean map produced by the GA-ILC on WMAP and Planck data with 1.15% mutation. Bottom: Difference map of GA-ILC and the SS-ILC. All the values are in  $\mu\text{K}$ . Notice that the residual contamination is very small and exists only close to the galactic plane. In other parts of the sky, a very good agreement can be seen.



**Figure 10.** The clean angular power spectrum produced by GA-ILC implemented on data with 1.15% mutation. The reconstruction errors in GA-ILC here are found using 200 Monte Carlo simulations. The two power spectra seem to agree quite well with each other.

that the minimal residual contamination is present in the GA-ILC clean map and that it tends to occupy small areas close to the galactic plane. The clean angular power spectrum calculated from the GA-ILC clean map (data implementation) is overplotted with SS-ILC clean power spectrum in fig. 10. We observe that the two match very well with each other. This also indicates that the purely numerical GA-ILC technique gives as good results as SS-ILC with analytical expression of weights.

We compare our GA-ILC results with those obtained by various component reconstruction methods of other science groups, namely, COMMANDER, NILC, SMICA (Planck Collaboration et al. 2020b), and WMAP-ILC (Bennett et al. 2013b). Shown in fig. 11 are the difference maps of each of those clean maps and the GA-ILC clean map (data implementation, of course). It is evident from here that our method produces a clean map that agrees well with some other completely different methods. We also observe that the residual contamination near the Milky Way plane is different in different methods. This indicates that those other clean maps also contain some (minimal) amount of residual foreground, same as ours. Finally we show, in fig. 12, each of the angular power spectra of GA-ILC and that of COMMANDER, NILC, SMICA, and WMAP-ILC for comparison. As expected, the spectra agree well with each other, with the small difference between all the different methods. Again, the other methods' results differ from each other same as our method's.

## 7 CONCLUSION

In this paper, for the first time in literature, we develop and implement the biological-selection-rule-motivated genetic algorithm to reconstruct the CMB component over large angular scales by removing foregrounds using linear combination of multifrequency observations of WMAP and Planck satellite missions. We validate our methodology by performing 200 Monte Carlo simulations using realistic observations from the final-year WMAP and Planck missions. The results of the simulations show that the CMB map and the angular power spectrum can be accurately recovered by using our method. The outcome of our method is in close agreement with the results obtained by using weights following the exact analytical method which demonstrates usefulness of the new method of this paper. We compare the cleaned CMB maps and recovered angular power spectrum obtained by the new method with those obtained by WMAP and Planck science groups. These results agree well with each other, which shows that the CMB results obtained by the satellite missions are robust with respect to the data analysis algorithms applied. Enriched in inherent parametric characteristics, GA-ILC is a very flexible and volatile method to work with. Nonetheless, since GA is expected to produce robust results with respect to fluctuations in the optimizing system, our method opens up a new avenue to apply the method when the weight factors for linear combination in a modified ILC method can no longer be obtained in a closed analytical form, e.g., when one is interested in an objective function which deviates from quadratic nature. The larger domain of application of the GA-ILC is a very promising feature and will be explored in the future communications by the authors.

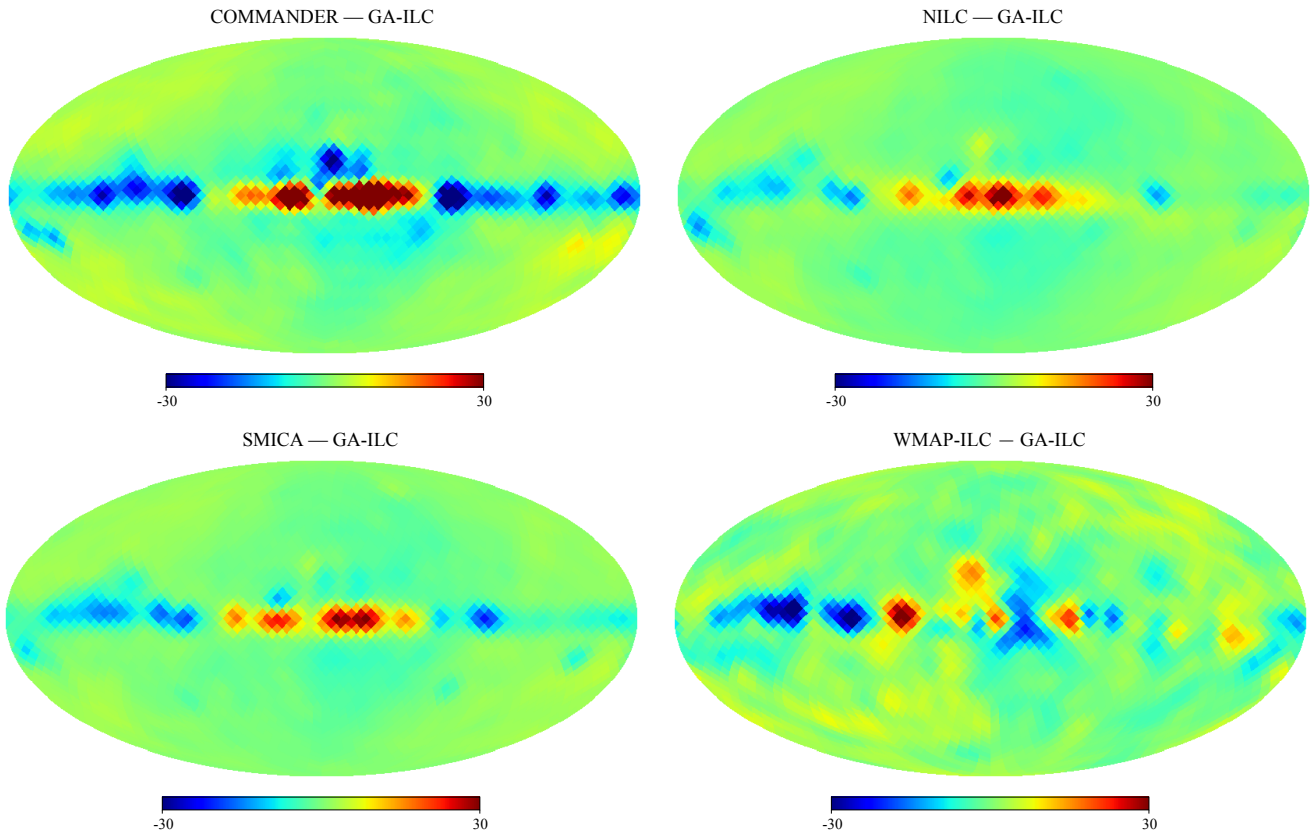


**Figure 11.** Difference maps of several other foreground reconstruction techniques and GA-ILC implemented on data. Notice that except the small residual foreground close to the galactic equator – which itself varies from one method to the other, our results agree very nicely with those of other methods. The values are in  $\mu\text{K}$ .

## ACKNOWLEDGEMENTS

We thank the HPC cluster facility, “Kanad” of IISER Bhopal for providing access and resources for the crucial part of this research.

## 8 DATA AVAILABILITY

The data pertaining to this article will be shared on reasonable request to the corresponding author.

## REFERENCES

- Acquaviva V., Bartolo N., Matarrese S., Riotto A., 2003, *Nuclear Physics B*, 667, 119
- Allen T., Grinstein B., Wise M. B., 1987, *Physics Letters B*, 197, 66
- Bennett C. L., et al., 2003a, *ApJS*, 148, 1
- Bennett C. L., et al., 2003b, *ApJS*, 148, 97
- Bennett C. L., et al., 2013a, *ApJS*, 208, 20
- Bennett C. L., et al., 2013b, *ApJS*, 208, 20
- Bouchet F. R., Gispert R., 1999, *New Astron.*, 4, 443
- Dodson S., 1997, *The Astrophysical Journal*, 482, 577
- Eriksen H. K., et al., 2004a, *The Astrophysical Journal Supplement Series*, 155, 227–241
- Eriksen H. K., Banday A. J., Gorski K. M., Lilje P. B., 2004b, *The Astrophysical Journal*, 612, 633
- Eriksen H. K., et al., 2006, *ApJ*, 641, 665
- Eriksen H. K., Huey G., Saha R., et al., 2007, *The Astrophysical Journal*, 656, 641
- Eriksen H. K., Dickinson C., Jewell J. B., Banday A. J., Górski K. M., Lawrence C. R., 2008a, *ApJ*, 672, L87
- Eriksen H. K., Jewell J. B., Dickinson C., Banday A. J., Górski K. M., Lawrence C. R., 2008b, *ApJ*, 676, 10
- Falk T., Rangarajan R., Srednicki M., 1992, *Phys. Rev. D*, 46, 4232
- Gangui A., Lucchin F., Matarrese S., Mollerach S., 1994, *ApJ*, 430, 447
- Geman S., Geman D., 1984, *IEEE Transactions on Pattern Analysis and Machine Intelligence*, PAMI-6, 721
- Gold B., et al., 2011, *ApJS*, 192, 15
- Goldberg D. E., 1989, *Genetic algorithms in search, optimization, and machine learning*. Addison-Wesley Publishing Company, Inc.
- Górski K. M., Hivon E., Banday A. J., Wandelt B. D., Hansen F. K., Reinecke M., Bartelmann M., 2005, *ApJ*, 622, 759
- Hinshaw G., et al., 2003, *ApJS*, 148, 135
- Hinshaw G., et al., 2007, *ApJS*, 170, 288
- Holland J. H., 1962, *J. ACM*, 9, 297–314
- Ichiki K., 2014, *Progress of Theoretical and Experimental Physics*, 2014
- Jarosik N., Bennett C. L., et al., 2003, *ApJS*, 145, 413
- Jarosik N., et al., 2007, *ApJS*, 170, 263
- Maldacena J., 2003, *Journal of High Energy Physics*, 2003, 013
- Mather J. C., et al., 1994, *ApJ*, 420, 439
- Moore E. H., 1920, *Proceedings of the American Mathematical Society*
- Penrose R., 1956, *Proceedings of the Cambridge Philosophical Society*, 52, 17

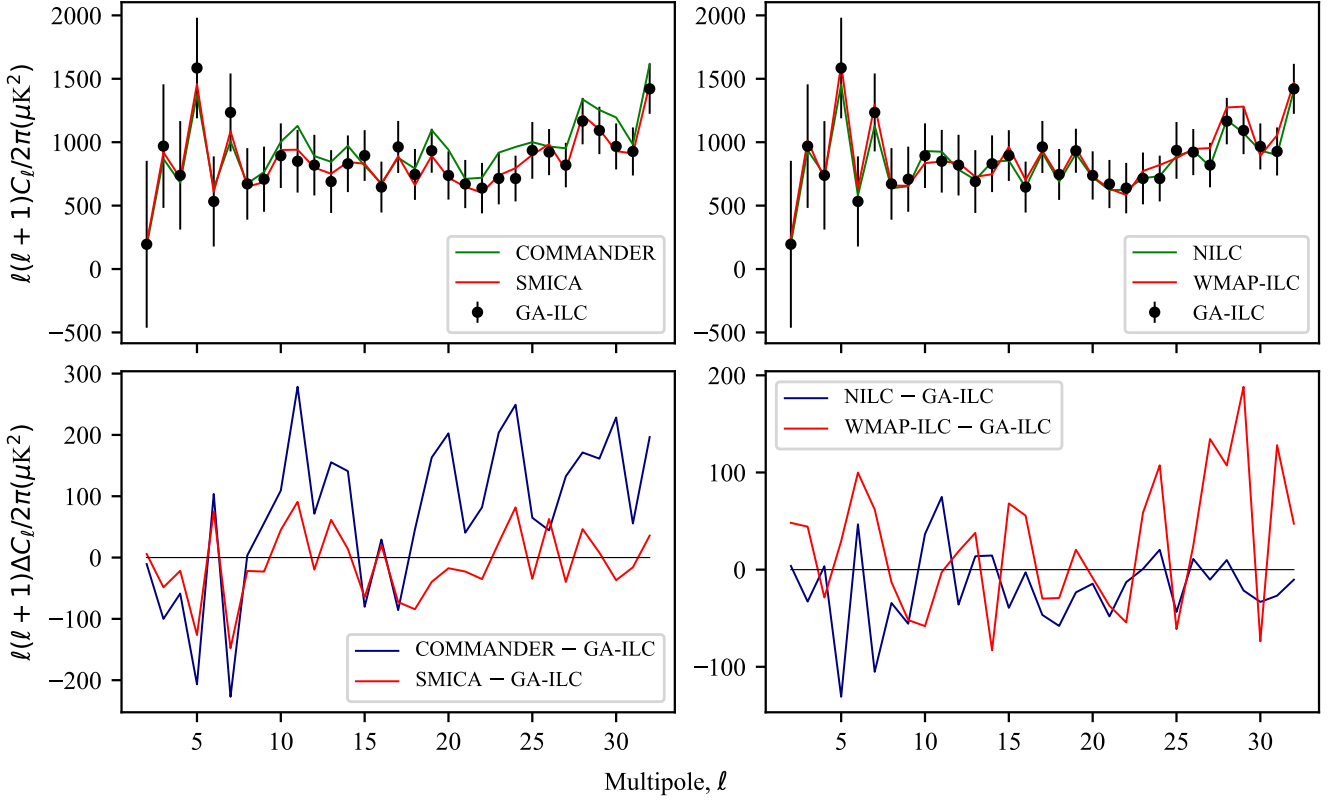


**Figure 12.** Comparison of angular power spectrum of the GA-ILC clean map with those of several different foreground reconstruction techniques. Bottom panel: differences of those various clean angular power spectra and GA-ILC clean power spectrum (data implementation). A good agreement between GA-ILC and other methods is seen here as well.

- Planck Collaboration et al., 2020a, *A&A*, 641, A1  
 Planck Collaboration et al., 2020b, *A&A*, 641, A4  
 Planck Collaboration et al., 2020c, *A&A*, 641, A6  
 Saha R., 2011, *The Astrophysical Journal*, 739, L56  
 Saha R., Jain P., Souradeep T., 2006, *The Astrophysical Journal*, 645, L89–L92  
 Saha R., Prunet S., Jain P., Souradeep T., 2008a, *Phys. Rev. D*, 78, 023003  
 Saha R., Prunet S., Jain P., Souradeep T., 2008b, *Phys. Rev. D*, 78, 023003  
 Sudevan V., Saha R., 2018a, An Application of Global ILC Algorithm over Large Angular Scales to Estimate CMB Posterior Using Gibbs Sampling ([arXiv:1810.08872](https://arxiv.org/abs/1810.08872))  
 Sudevan V., Saha R., 2018b, arXiv e-prints, p. [arXiv:1810.08872](https://arxiv.org/abs/1810.08872)  
 Sudevan V., Saha R., 2018c, *The Astrophysical Journal*, 867, 74  
 Tegmark M., 1998, *ApJ*, 502, 1  
 Tegmark M., Efstathiou G., 1996, *Monthly Notices of the Royal Astronomical Society*, 281, 1297–1314  
 Tegmark M., de Oliveira-Costa A., Hamilton A. J. S., 2003, *Physical Review D*, 68

This paper has been typeset from a  $\text{\TeX}/\text{\LaTeX}$  file prepared by the author.